Fatigue behaviour assessment of ductile cast iron smooth specimens

Submitted to INTERNATIONAL JOURNAL OF FATIGUE

Special Issue "1st Virtual European Conference on Fracture (VECF1)"

February 2021

REVISED VERSION JULY 2021

FATIGUE BEHAVIOUR ASSESSMENT OF DUCTILE CAST IRON SMOOTH SPECIMENS

Sabrina Vantadori[a], Camilla Ronchei[b], Daniela Scorza[c],

Andrea Zanichelli[a], Andrea Carpinteri[a]

[a] Department of Engineering & Architecture, University of Parma,
Parco Area delle Scienze 181/A, 43124 Parma, Italy

[b] Department of Civil Engineering, University of Calabria,
via Pietro Bucci, 87036 Arcavacata di Rende (CS), Italy

[c] Department of Engineering, University of Naples Parthenope,
Centro Direzionale Isola C4, 80143 Napoli, Italy

Corresponding author: camilla.ronchei@unical.it

ABSTRACT

In the present paper, the fatigue behaviour of two Ductile Cast Irons (DCIs) is analyzed. Both infinite and finite life fatigue tests are simulated by employing the Carpinteri et al. criterion. Such tests, found in the literature, are related to DCI smooth specimens subjected to proportional and non-proportional constant amplitude cyclic loadings. The theoretical results are compared with the experimental ones in terms of both fatigue endurance and fatigue life.

KEYWORDS: critical plane approach; Ductile Cast Iron; fatigue endurance; fatigue life; uniaxial/biaxial loading.

1. INTRODUCTION

Cast irons are the most important casting materials (accounting for about 70% of the total world casting tonnage) due to their interesting combination of mechanical and technological properties. Moreover, the widespread use of such materials in several applications is also justified by their competitive price. Crankshafts, camshafts, pistons, cylinders, heavy sections of wind turbine components, railway brake disks, wheels are only a few examples of cast iron industrial applications **[1]**.

Although cast irons have been used for thousands of years (dating back to 500 B.C. in China), the discovery of Ductile Cast Iron (DCI) occurred in the forties and gave a new lease of life to the cast iron family. Until then, indeed, only long and expensive heat treatments had been performed on white cast iron (that is, cast iron containing carbides) in order to obtain the so-called malleable cast iron, characterised by a combination of good castability and high toughness values. Since 1943, the simple addition of controlled amounts of magnesium or cerium to iron melt, prior to cast, made it possible to obtain a new cast iron containing nearly perfect graphite spheres (i.e. Ductile Cast Iron or Spheroidal Graphite Iron, SGI). Such a cast iron was characterised by both the same mechanical properties of the malleable cast iron and reduced production costs **[2,3]**.

As has been previously mentioned, DCIs are able to combine the main advantages of cast irons (such as good castability and excellent machinability) with steel mechanical properties (e.g. high

mechanical strength, remarkable fatigue resistance, toughness, hardenability, ductility and hot workability) **[4]**. Note that the DCI mechanical properties depend on both the matrix microstructure, the graphite morphology (shape, dimension, distribution, volume fraction) and the presence of defects (inclusions, porosity, degenerate graphite).

The matrix microstructure depends on the cooling cycles from the annealing temperature, and the matrix name is commonly used to designate the different types of DCIs (that is, ferritic, pearlitic, martensitic, bainitic, austenitic and austempered DCIs) **[5]**. As an example, ferritic matrix is characterised by high ductility and limited tensile strength, whereas pearlitic matrix gives the material very high strength, good wear resistance but moderate ductility **[6]**. Note that solution strengthened ferritic DCIs have been recently developed in order to improve their mechanical properties with respect to traditional ferritic-pearlitic DCIs. The static and fatigue properties of such innovative DCIs, characterised by a very long solidification time, have been recently examined by Borsato et al. **[7]**.

As far as graphite elements (also named graphite nodules) are concerned, it is well-known that their morphology has a significant influence on both the mechanical behaviour (see for instance Ref. **[8]**) and the thermal response **[9]** of DCIs, and also plays a fundamental role in the crack initiation and propagation processes **[10]**. Regarding the latter aspect, the analysis of the graphite nodule influence on DCI damaging mechanisms is not a trivial issue,

since such mechanisms depend on both the loading conditions (static, quasi-static, cyclic, dynamic loading) and the matrix microstructure **[11].** Consequently, a lot of effort has been made by the Scientific Community to better examine the different failure mechanisms occurring in DCI specimens **[12-14].** In such a context, the systematic experimental investigation performed by Iacoviello et al. **[15-18]** certainly deserves to be mentioned.

Under cyclic loading, the influence of both the graphite nodules and matrix microstructure on fatigue crack mechanisms has not been univocally determined. Consequently, this research topic is still open and worthy of investigation **[19-21].** For instance, by only analyzing the most recent published papers, Hosdez et al. have employed a projective digital image correlation method to identify a crack propagation law for DCI specimens under Mode I cyclic loading **[22].** The fatigue damage mechanisms of a ferritic DCI under multiaxial non-proportional cyclic loading have been experimentally and analytically examined by Kachit and Verdue **[23].** Further, the overload influence on crack propagation mechanisms of fatigue pre-cracked specimens (made of a ferritic-pearlitic DCI) has been experimentally investigated by Iacoviello et al. **[24].** The effects of both graphite morphology and ferritic nitrocarburizing on the corrosion-fatigue behaviour of a ferritic DCI have been also discussed in Refs. **[25,26].**

In the present paper, the High Cycle Fatigue (HCF) behaviour of DCI specimens under both uniaxial and biaxial cyclic loading is theoretically examined. In particular, several sets of fatigue tests

available in the literature **[27-29]** are hereafter simulated by applying the critical plane-based multiaxial fatigue criterion proposed by Carpinteri et al. (Ref. **[30]**). Note that the fatigue behaviour of DCI smooth specimens has been recently evaluated through such a criterion for fatigue tests performed in the finite life regime **[31,32]**. The novelty of the present paper is to also model infinite life tests (where the number of loading cycles is considered "infinite" when it varies between approximately 1 to 100 million). Another novelty aspect of the present paper is related to the material investigated. In more detail, the accuracy of the Carpinteri et al. criterion has been extensively assessed by taking into account steels, aluminium alloys and gray cast irons, whereas no simulations involving DCIs have been so far performed.

The basic concepts of such a multiaxial fatigue criterion are outlined in Sections 2. Then, the examined infinite and finite life tests are discussed in Section 3. The effectiveness of the above criterion is evaluated in Section 4 and, finally, some conclusions are drawn in Section 5.

2. FUNDAMENTALS OF THE CARPINTERI ET AL. CRITERION

The multiaxial fatigue criterion here employed to theoretically examine the fatigue behaviour of DCI smooth specimens is that proposed by Carpinteri et al. **[30]**. Such a criterion, based on the so-called critical plane approach, allows us to estimate the fatigue strength or fatigue life of metallic structural components under

both proportional and non-proportional constant amplitude cyclic loadings. The criterion is formulated in terms of stresses for High-Cycle Fatigue (HCF) regime. Its flowchart is shown in **Figure 1**.

First of all, some material fatigue properties have to be set: the fatigue strengths $\sigma_{af,-1}$ and $\tau_{af,-1}$ under fully reversed normal stress and shear stress, respectively; the inverse slopes k and k^* related to the S-N curves under fully reversed normal stress and shear stress, respectively; the ultimate tensile strength σ_u.

Figure 1

Subsequently, by considering the stress tensor at the material point P of a structural component, the fatigue strength assessment is performed on a verification plane, named critical plane, which is determined by using a two-step procedure:

(i) computation of averaged principal stress directions $\hat{1},\hat{2},\hat{3}$ at point P, by employing a suitable weight function;

(ii) determination of the vector $\mathbf{w}$, normal to the critical plane, which is linked to the averaged maximum principal stress direction $\hat{1}$.

Details on the procedure employed for critical plane determination are reported in **Appendix A**.

Once the critical plane is identified, a local frame $Puvw$ is adopted:

- the u-direction is represented by the intersection line between the critical plane and the plane defined by $\mathbf{w}$ and Z-axis;
- the v-direction forms an orthogonal frame with u and w.

The normal, $\mathbf{N}$, and shear, $\mathbf{C}$, components of the stress vector $\mathbf{S_w}$, related to the above local frame, are computed at each time instant of the fatigue loading history. During a loading cycle, the direction of $\mathbf{N}$ is fixed with respect to time and, consequently, its amplitude N_a and mean value N_m are readily evaluated. Conversely, the amplitude C_a of the shear stress vector is not uniquely defined, since the direction of $\mathbf{C}$ is time-varying. In the present paper, the Maximum Rectangular Hull (MRH) method **[33]** is adopted for the computation of C_a.

Then, the fatigue endurance condition can be quantified by equating the equivalent uniaxial stress amplitude $\sigma_{eq,a}$ to the fatigue strength $\sigma_{af,-1}$:

$$\sigma_{eq,a} = \sqrt{N_{eq,a}^2 + \left(\frac{\sigma_{af,-1}}{\tau_{af,-1}}\right)^2 C_a^2} = \sigma_{af,-1} \tag{1}$$

with

$$N_{eq,a} = N_a + \sigma_{af-1}\left(\frac{N_m}{\sigma_u}\right) \tag{2}$$

Finally, by exploiting the Basquin relationships for both fully reversed normal stress ($\sigma'_{af,-1} = \sigma_{af,-1}(N_{cal}/N_0)^k$) and fully reversed shear stress ($\tau'_{af,-1} = \tau_{af,-1}(N_{cal}/N_0)^{k^*}$), we get:

$$\sigma_{eq,a}=\sqrt{N_{eq,a}^2+\left(\frac{\sigma_{af,-1}}{\tau_{af,-1}}\right)^2\left(\frac{N_{cal}}{N_0}\right)^{2k}\left(\frac{N_0^*}{N_{cal}}\right)^{2k^*}C_a^2}=\sigma_{af,-1}\left(\frac{N_{cal}}{N_0}\right)^k \quad (3)$$

where N_0 and N_0^* are the reference numbers of loading cycles under fully reversed normal stress and shear stress, respectively. In practice, it is reasonable to consider $N_0=N_0^*=2\cdot10^6$. The above equation provides the number of loading cycles to failure, N_{cal}, by performing an iterative procedure.

3. UNIAXIAL AND MULTIAXIAL FATIGUE DATA EXAMINED

The Carpinteri et al. criterion is here applied to some fatigue tests (Refs **[27-29]**) on smooth specimens made of DCIs, subjected to constant amplitude uniaxial and biaxial loading. In particular, the data related to both infinite **[27,28]** and finite life tests **[29]** are examined in the following Sub-Sections.

3.1 Infinite life fatigue tests

Regarding infinite life tests, the experimental campaign reported in Refs **[27,28]** is characterised by a number of loading cycles mostly greater than $1\cdot10^6$ cycles.

The investigated material is a commercial DCI, identified as EN-GJS-700-2, with a pearlitic matrix and uniformly distributed spheroidal graphite nodules. The metallographic examination was performed by using an optical microscope and a SEM, proving that the microstructure was fully pearlitic. Moreover, graphite nodules, intercellular carbides and shrinkage porosity were also observed.

The formation of shrinkage porosity (i.e. metallurgical defect) is mainly due to the excess content of both molybdenum and phosphorus. Note that molybdenum is added to favour the formation of spheroidal graphite, whereas the addition of phosphorus allows to increase the fluidity of the molten state during casting.

In order to improve the fatigue properties of DCI EN-GJS-700-2, a stress relieving heat treatment process was performed, thus eliminating tensile residual stresses left from manufacturing processes.

The experimental data are related to constant amplitude uniaxial and biaxial cyclic loadings. The sequences of such loadings were applied according to the staircase method **[27]**. Uniaxial fatigue tests, as well as biaxial ones, were conducted under load control on small cylindrical smooth specimens. Such specimens, cut from large section of DCI, were characterised by different diameters of the gauge section, namely 7 mm for tensile tests and 16 mm for torsional and biaxial ones. The geometrical sizes of the specimens subjected to torsional and biaxial loading are shown in **Figure 2(a)**.

Figure 2

Regarding tensile fatigue tests, a Rumul machine with a maximum load up to ±50 kN was used, whereas torsional and biaxial tests were performed by means of a servo-hydraulic biaxial test system (Walter + Bai LFV250–T2200, with axial load up to 250 kN and torques up to 2200 Nm with a ±50° torsional angle).

The uniaxial fatigue tests were performed under fully reversed tension or fully reversed torsion (i.e., $R=-1$). In the biaxial tests, the specimens were subjected to a pulsating compression and an alternating torsion with a phase shift β equal to 90°.

Each specimen was assumed to fail when a visible crack appeared during the experiment, whereas the run-out condition was defined in correspondence to a number of loading cycles equal to 10^7 cycles.

The experimental data here examined are reported in **Tables 1-3**, where σ and τ are the applied normal and shear stresses, respectively. Moreover, the subscripts a and m refer to amplitude and mean value of the above stresses, respectively. The experimental number of cycles to failure, N_{exp}, for each specimen is also listed in **Tables 1-3**.

Table 1

Table 2

Table 3

From uniaxial data (**Tables 1,2**), the fully reversed fatigue strengths (that is, $\sigma_{af,-1}$ and $\tau_{af,-1}$), computed through the method of Hodge-Rosenblatt (for more details, see Ref. **[27]**), are reported in **Table 4**. Since the ultimate tensile strength σ_u was not measured during the experimental campaign, its value (listed in **Table 4**) is taken from Ref. **[34]**.

Table 4

After fatigue tests, all surfaces of the broken specimens were examined by means of SEM, observing that fatigue cracks nucleated from the largest surface of the shrinkage porosity, which behaved as a stress riser. Then, cracks propagated towards the specimen surface.

3.2 Finite life fatigue tests

Regarding finite life tests, the experimental campaign reported in Ref. **[29]** is characterised by a number of loading cycles between 10^4 and $3 \cdot 10^6$ cycles.

The investigated material is a commercial DCI, identified as EN-GJS-400-18, with ferritic matrix and spheroidal graphite nodules. From the microstructural investigation, the following averaged properties were obtained: nodule count equal to ≈50 nod. No./mm^2 (x 100), nodularity equal to ≈80÷85%, average nodule size equal to ≈50μm, and ferritic content equal to ≈90%. Accordingly, the quality of the investigated DCI was considered sufficiently good, as is proved by the high ratio of the graphite nodularity.

The experimental data are related to constant amplitude uniaxial and biaxial cyclic loadings. In particular, both uniaxial and multiaxial fatigue tests were performed under load control on small cylindrical smooth specimens, with a gauge section diameter equal to 12.5 mm (see **Figure 2 (b)**). Such specimens were produced by

coring a very large structural component in a potential critical zone.

For tensile fatigue tests, a MTS 810 servo-hydraulic testing machine with a 250kN axial load cell was used, whereas torsional and biaxial tests were performed by means of a MTS 809 servo-hydraulic biaxial testing machine with a 100kN axial load cell and a 1100Nm torsional load cell.

The tensile fatigue tests were carried out by considering both positive and negative mean values of the applied stress (that is, $R = 0.5, 0, -3$). Moreover, fully reversed tensile loading (i.e. $R = -1$) was also applied. In the torsional fatigue tests, the loading mean value ranged from a positive value (for $R = 0$) to zero (for $R = -1$). Finally, in the biaxial tests, the specimens were subjected to both fully reversed tensile and torsional loading with a phase shift β equal to 0° or 90°.

Each specimen was assumed to fail when its complete separation occurred during the fatigue test, whereas the run-out condition was defined at a number of loading cycles equal to about $3 \cdot 10^6$ cycles.

The details of the experimental loading conditions are reported in Refs **[29,32]**. Moreover, the material fatigue properties (listed in **Table 4**) were computed from uniaxial data, whereas the value of σ_u was adopted according to the DCI designation.

After fatigue tests, no clear and unique evidence was obtained as far as the crack nucleation direction was concerned, since it strictly depended on both microstructural properties and local defect distribution (for more details, see **Ref. [29]**).

4. CRITERION VALIDATION: DISCUSSION OF RESULTS

In order to assess the Carpinteri et al. criterion accuracy in estimating fatigue endurance, both infinite and finite life fatigue tests (described in Section 3) have been simulated. In particular, the fatigue endurance condition, given by Eq.(1), is illustrated by the C_a against $N_{eq,a}$ diagram, reported in **Figures 3** and **4** for infinite life tests and in **Figure 5** for finite life tests.

Accordingly, each point $(N_{eq,a},C_a)$ in these diagrams represents the stress level associated with a given experimental test, whereas Eq.(1) defines the ellipse with semi-axis equal to $\sigma_{af,-1}$ and $\tau_{af,-1}$. Fatigue failure occurs if point $(N_{eq,a},C_a)$ lies out of the elliptical domain, whereas the safe domain is located inside the elliptical domain.

It can be highlighted that different tests carried out at the same stress level are represented by only one point in the C_a against $N_{eq,a}$ diagram, according to the Carpinteri et al. criterion. Moreover, if such tests experimentally show both failures and run-outs, the criterion should predict the most conservative condition (that is, failure of the specimen) in order to be regarded as a powerful engineering tool in fatigue design.

For uniaxial fatigue tests at infinite life (see **Figure 3(a)** for tensile loading, and **Figure 3(b)** for torsional loading), the above

criterion estimates failure for tests No. T1 and No. T4, in agreement with the experimental observations (see **Tables 1** and **2**). On the other hand, the experimental data points corresponding to tests T11 and T16-T18 fall inside the elliptical domain, in agreement with the experimental run-outs. The data points corresponding to tests T5-T6 and T12-T15 should be located outside the ellipse, since failures were observed. However, such points lie very close to the failure curve and, consequently, the criterion allows to estimate a condition of incipient failure. Finally, for tensile tests T2-T3, T7-T8 and T9-T10, which experimentally showed both failures and run-outs (**Table 1**), the criterion is able to predict the failure condition only for test T2-T3. However, data points corresponding to tests T7-T8 and T9-T10 are very close to the ellipse within the error band equal to $\pm 20\%$ (see the dashed lines in **Figure 3(a)**).

Figure 3

For biaxial fatigue tests at infinite life (**Figure 4**), the above criterion estimates run-outs for tests No. T35 and No. T36, in agreement with the experimental results. For biaxial tests T19, T20-23 and T24-26, the data points lie very close to the ellipse, that is to say, the criterion does not estimate the experimental failures, but rather a condition of incipient failure. Note that, since tests T20-23 are characterised by a large dispersion in terms of N_{exp} values, the accuracy of the result obtained by means of the criterion is difficult to be discussed. Finally, non-conservative

predictions (that is, run-outs) are obtained for tests T27-T30 and T31-T34, even if failures of some specimens were observed.

Figure 4

For uniaxial and biaxial fatigue tests at finite life (**Figure 5**), the criterion estimates failure for almost all tests, in agreement with the experimental outcomes. The data points falling inside the elliptical domain correctly represent experimental run-outs.

Figure 5

Regarding the finite life fatigue tests, the Carpinteri et al. criterion allows to estimate the number N_{cal} of loading cycles to failure. In particular, N_{cal} is calculated through Eq. (3) for all fatigue data presented in Sub-Section 3.2, with the exception of those related to run-out conditions.

The comparison between experimental, N_{exp}, and estimated, N_{cal}, fatigue life is shown in **Figure 6**. Note that the dashed lines correspond to scatter band 2x, i.e. $N_{cal}/N_{exp}=2$ and $1/2$, and the dash-dot lines correspond to scatter band 3x, i.e. $N_{cal}/N_{exp}=3$ and $1/3$.

From such graphs, it can be observed that:

(i) for tensile fatigue loading (**Figure 6(a)**), 82% of the results fall within the scatter band 2x, whereas 100% of the results fall within the scatter band 3x;

(ii) for torsional fatigue loading (**Figure 6(b)**), 60% of fatigue life calculations are included into scatter band 2x, whereas 90% of such calculations are included into scatter band 3x;

(iii) for biaxial fatigue loading (**Figure 6(c)**), 36% of the results fall within the scatter band 2x, whereas 100% of the results fall within the scatter band 3x.

Figure 6

Further considerations on the accuracy of the Carpinteri et al. criterion in estimating the fatigue life can be also made by examining the values of the mean square error defined as follows:

$$T_{RMS} = 10^{E_{RMS}} \tag{4}$$

where E_{RMS} is given by:

$$E_{RMS} = \sqrt{\frac{\sum_{i=1}^{j} \log^2 \left(N_{exp} / N_{cal} \right)_i}{j}} \tag{5}$$

being j the number of fatigue data being examined. According to Eq. (4), if all the calculated results fell within the scatter band 3x, the value of T_{RMS} would be lower than 3.

Figure 7 shows the T_{RMS} value computed for the different loading conditions here examined. In particular, such a value is always lower than 3, proving that the agreement between experimental and

calculated fatigue lives is satisfactory, independent of the loading condition (that is, both proportional and non-proportional uniaxial and biaxial loading).

Figure 7

5. CONCLUSIONS

In the present paper, the HCF behaviour of DCI smooth specimens is theoretically examined. In particular, several sets of uniaxial and biaxial fatigue tests available in the literature have been simulated through the critical plane-based fatigue criterion proposed by Carpinteri et al. **[30]**.

The experimental results herein analyzed are related to both infinite and finite life fatigue tests performed on DCI EN-GJS-700-2 and DCI EN-GJS-400-18 smooth specimens, respectively. Both proportional and non-proportional cyclic loadings have been investigated.

By means of the above criterion, an accurate evaluation of the fatigue endurance condition is achieved for both materials here examined.

Moreover, regarding the finite life fatigue tests, the results in terms of number of loading cycles to failure are satisfactory, falling into scatter band 3x and being the mean value of T_{RMS} equal to about 2.11.

Based on such encouraging results, it can be pointed out that the above criterion correctly simulates the fatigue behaviour of DCI

specimens. As future perspectives of this research work, the influence of metallurgical defects, dislocated in DCI specimens, on the definition of the proper fatigue strength values will be assessed.

Acknowledgements

The work of Sabrina Vantadori, Andrea Carpinteri and Andrea Zanichelli is supported by Italian Ministry of University and Research (P.R.I.N. National Grant 2017, Project code 2017HFPKZY; University of Parma Research Unit).

REFERENCES

[1] Iacoviello F, Di Cocco V. Influence of the graphite elements morphology on the fatigue crack propagation mechanisms in a ferritic ductile cast iron. Eng Fract Mech 2016;167:248-258.

[2] Ward RG. An introduction to the physical chemistry of iron and steel making. London: Arnold; 1962.

[3] Theuwissen K, Lacaze J, Laffont-Dantras L. Structure of graphite precipitates in cast iron. Carbon 2016;96:1120-1128.

[4] Gouveia RM, Silva FJG, Paiva OC, De Fátima Andrade M, Pereira LA, Moselli PC, Papis KJM. Comparing the Structure and Mechanical Properties of Welds on Ductile Cast Iron (700 MPa) under Different Heat Treatment Conditions. Metals 2018;8:72.

[5] Iacoviello F, Di Bartolomeo O, Di Cocco V, Piacente V. Damaging micromechanisms in ferritic–pearlitic ductile cast irons. Mater Sci Eng A 2008;478:181-186.

[6] Davis JR. Classification and basic metallurgy of cast irons. American Society of Metals. ASM specialty handbook cast iron. Illinois: ASTM; 1996, p. 4–17.

[7] Borsato T, Ferro P, Fabrizi A, Berto F, Carollo C. Long solidification time effect on solution strengthened ferritic ductile iron fatigue properties. Int J Fatigue 2021;145:106137.

[8] Lampic M. A new opportunity for cast iron with compacted graphite. Giesserei 1992;79:871–8.

[9] Angus HT. Cast iron: physical and engineering properties. London: Butterworth-Heinemann; 2013.

[10] Shikida M, Sakane M, Ohnami M. Fatigue crack propagation for cast iron rotating disk. JSME Int J Ser A Mech Mater Eng 1995;38:104–10.

[11] Dong M, Hu G, Diboine A, Moulin D, Prioul C. Damage modelling in nodular cast iron. J. de Physique IV 1993;03:43–648.

[12] Feaugas X, Clavel M. Mechanical behavior and damage kinetics in nodular cast iron: part I. Damage mechanisms. Metall Mater Trans A 2000;31:3063–3074.

[13] Andriollo T, Thorborg J, Hattel J. Modeling the elastic behavior of ductile cast iron including anisotropy in the graphite nodules. Int J Solids Struct 2016;100–101:523–35.

[14] Andriollo T, Hattel J. On the isotropic elastic constants of graphite nodules in ductile cast iron: analytical and numerical micromechanical investigations. Mech Mater 2016;96:138–50.

[15] Di Cocco V, Iacoviello F, Cavallini M. Damaging micromechanisms characterization of a ferritic ductile cast iron. Eng Fract Mech 2010;77:2016–2023

[16] De Santis A, Iacoviello D, Di Cocco V, Iacoviello, F. Graphite nodules features identification and damaging micromechanims in ductile irons. Frat ed Integrità Strutt 2013;26:12–21.

[17] Di Cocco V, Iacoviello F, Rossi A, Iacoviello D. Macro and microscopical approach to the damaging micromechanisms analysis in a ferritic ductile cast iron. Theor Appl Fract Mech 2014;69:26–33.

[18] Iacoviello F, Di Cocco V, Rossi A, Cavallini M. Damaging Micromechanisms Characterization in Pearlitic Ductile Cast Irons. Procedia Mater Sci 2014;3:295-300.

[19] Greno GL, Otegui JL, Boeri RE. Mechanisms of fatigue crack growth in Austempered Ductile Iron. Int J Fatigue 1999;21:35-43.

[20] Iacoviello F, Di Cocco V, Bellini C. Fatigue crack propagation and damaging micromechanisms in Ductile Cast Irons. Int J Fatigue 2019;124:48-54.

[21] Kihlberg E, Norman V, Skoglund P, Schmidt P, Moverare J. On the correlation between microstructural parameters and the thermo-mechanical fatigue performance of cast iron. Int J Fatigue 2021;145:106112.

[22] Hosdez J, Limodin N, Najjar D, Witz J-F, Charkaluk E, Osmond P, Forré A, Szmytka F. Fatigue crack growth in compacted and spheroidal graphite cast irons. Int J Fatigue 2020;131:105319

[23] Kachit M, Verdu C. Cracking behavior in nodular graphite cast iron under non-proportional cyclic loading. Int J Fatigue 2020;140:105840.

[24] Iacoviello F, Di Cocco V, Bellini C. Overload effects on fatigue cracks in a ferritized ductile cast iron. Int J Fatigue 2019;127:376-381.

[25] Xiang S, Hedström P, Zhu B, Linder J, Odqvist J. Influence of graphite morphology on the corrosion-fatigue properties of the ferritic Si-Mo-Al cast iron SiMo1000. Int J Fatigue 2020;140:105781.

[26] Xiang S, Jonsson S, Hedström P, Zhu B, Odqvist J. Influence of ferritic nitrocarburizing on the high-temperature corrosion-fatigue properties of the Si-Mo-Al cast iron SiMo1000. Int J Fatigue 2021;143:105984.

[27] Cengiz C. Out of Phase Multiaxial Fatigue Strength of a Cast Iron (Master thesis). Milan, Politecnico di Milano, 2012.

[28] Cristea ME, Foletti S, Cengiz C. Out of phase multiaxial fatigue strength of cast iron. Proceedings of the Tenth International Conference on Multiaxial Fatigue & Fracture (ICMFF10), Kyoto (Japan), 2013.

[29] Tovo R, Lazzarin P, Berto F, Cova M, Maggiolini E. Experimental investigation of the multiaxial fatigue strength of ductile cast iron. Theor Appl Fract Mech 2014;73:60-67.

[30] Vantadori S, Carpinteri A, Luciano R, Ronchei C, Scorza D, Zanichelli A, Okamoto Y, Saito S, Itoh T. Crack initiation and life

estimation for 316 and 430 stainless steel specimens by means of a critical plane approach. Int J Fatigue 2020;138:105677.

[31] Vantadori S, Carpinteri A, Ronchei C, Scorza D, Zanichelli A. Total life approach analysis of ductile cast iron smooth specimens. Procedia Struct Integr 2020;28:1055-1061.

[32] Vantadori S, Ronchei C, Zanichelli A, Scorza D. Fatigue life assessment of DCI smooth specimens. Mat Design Process Comm 2020;e210:1-9.

[33] Araújo JA, Dantas AP, Castro FC, Mamiya EN, Ferreira JLA. On the characterization of the critical plane with a simple and fast alternative measure of the shear stress amplitude in multiaxial fatigue. Int J Fatigue 2011;33:1092-100.

[34] Bauccio ML. ASM Metals Reference Book. Materials Park, Ohio: ASM International; 1993

NOMENCLATURE

C_a	amplitude of the shear stress component on the critical plane
k	inverse slope of the S-N curve under fully reversed normal stress
k^*	inverse slope of the S-N curve under fully reversed shear stress
N_a	amplitude of the normal stress component perpendicular to the critical plane
N_{cal}	calculated number of loading cycles to failure
$N_{eq,a}$	equivalent normal stress amplitude
N_{exp}	experimental number of loading cycles to failure
N_m	mean value of the normal stress component perpendicular to the critical plane
N_0	reference number of loading cycles under fully reversed normal stress
N_0^*	reference number of loading cycles under fully reversed shear stress
Puvw	local frame attached to the critical plane
$\mathrm{P}\hat{1}\hat{2}\hat{3}$	averaged principal stress frame
R	loading ratio
T_{RMS}	mean square error value
$\mathbf{w}$	normal vector to the critical plane
β	phase shift between normal stress and shear stress
σ	applied normal stress
$\sigma_{af,-1}$	material fatigue strength under fully reversed normal stress
$\sigma_{eq,a}$	equivalent uniaxial stress amplitude
σ_u	material ultimate tensile strength
τ	applied shear stress
$\tau_{af,-1}$	material fatigue strength under fully reversed shear stress

Subscripts

a	amplitude
m	mean value

Appendix A – Critical plane orientation according to the Carpinteri et al. criterion

The determination of the critical plane orientation according to the procedure proposed by Carpinteri and co-workers **[30]** is here explained.

Let us consider the stress state at point P of a generic structural component, for a generic time instant t of the fatigue loading history. The principal stresses σ_1, σ_2 and σ_3 (with $\sigma_1 \geq \sigma_2 \geq \sigma_3$) and the corresponding principal stress directions 1, 2 and 3 (identified by means of the principal Euler angles ϕ, θ and ψ) can be computed. Since the principal directions are generally time-varying under multiaxial fatigue loading, Carpinteri et al. suggested to evaluate the averaged principal stress directions $\hat{1}, \hat{2}$ and $\hat{3}$ by averaging the principal Euler angles on one cyclic loading period T:

$$\hat{\phi} = \frac{1}{W}\int_0^T \phi(t)\, W(t)\, dt$$

$$\hat{\theta} = \frac{1}{W}\int_0^T \theta(t)\, W(t)\, dt \qquad \text{(A.1)}$$

$$\hat{\psi} = \frac{1}{W}\int_0^T \psi(t)\, W(t)\, dt$$

where $W(T)$ is the weight function expressed by

$$W(t)=\begin{cases}0, & \sigma_1(t)<\sigma_{1,max}\\ 1, & \sigma_1(t)=\sigma_{1,max}\end{cases} \tag{A.2}$$

being $\sigma_{1,max}$ the maximum value achieved by $\sigma_1(t)$ during T.

The unit vector $\mathbf{w}$, normal to the critical plane, is assumed to be linked to the $\hat{1}$-direction through an off-angle δ, computed by the following empirical expression:

$$\delta=\frac{3\pi}{8}\left[1-\left(\frac{\tau_{af,-1}}{\sigma_{af,-1}}\right)^2\right] \tag{A.3}$$

Such a rotation δ is generally performed in the $\hat{1}\hat{3}$ plane, where $\hat{1}$ and $\hat{3}$ are the averaged directions of maximum and minimum principal stress, respectively.

Submitted to INTERNATIONAL JOURNAL OF FATIGUE

Special Issue "1st Virtual European Conference on Fracture (VECF1)"

February 2021

REVISED VERSION JULY 2021

FATIGUE BEHAVIOUR ASSESSMENT OF DUCTILE CAST IRON SMOOTH SPECIMENS

Sabrina Vantadori[a], Camilla Ronchei[b], Daniela Scorza[c],

Andrea Zanichelli[a], Andrea Carpinteri[a]

[a] Department of Engineering & Architecture, University of Parma,
Parco Area delle Scienze 181/A, 43124 Parma, Italy

[b] Department of Civil Engineering, University of Calabria,
via Pietro Bucci, 87036 Arcavacata di Rende (CS), Italy

[c] Department of Engineering, University of Naples Parthenope,
Centro Direzionale Isola C4, 80143 Napoli, Italy

Corresponding author: camilla.ronchei@unical.it

FIGURES AND TABLES

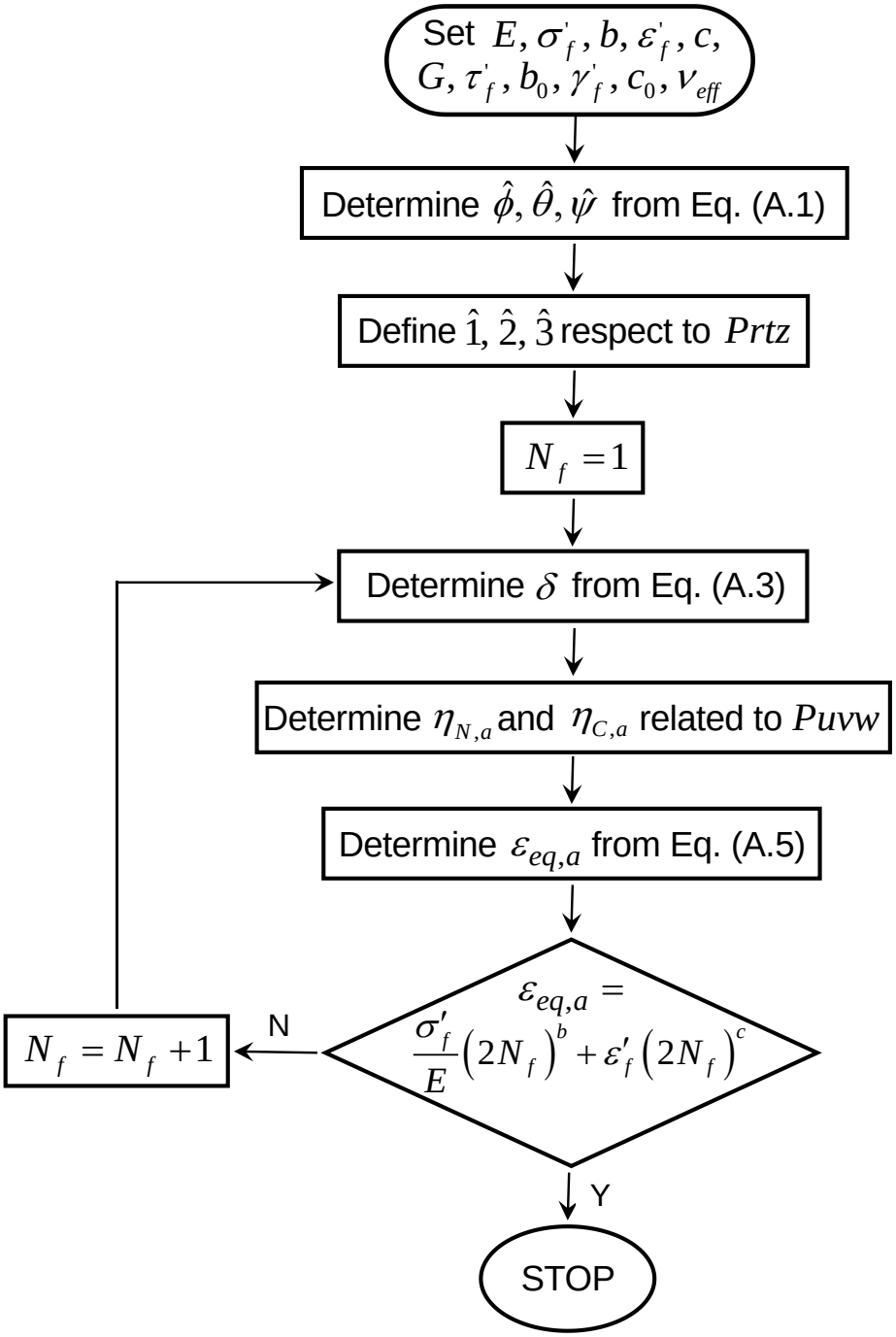

Figure 1. Flowchart of the critical plane-based criterion by Carpinteri et al. **[30].**

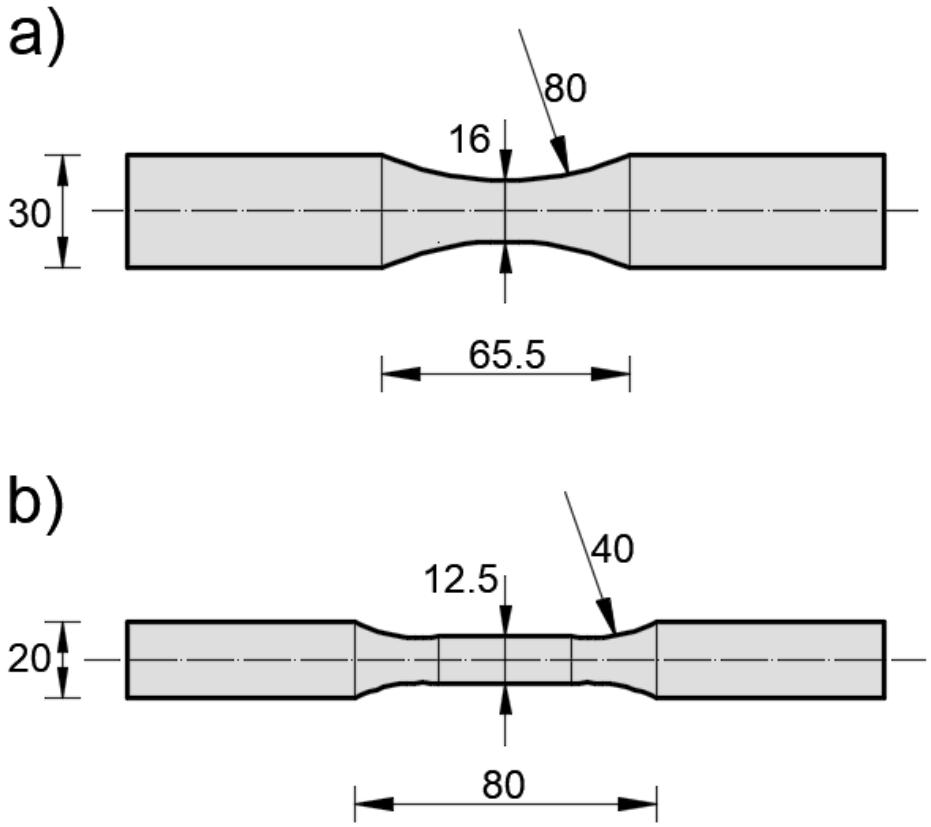

Figure 2. Geometrical sizes (expressed in mm) of specimens subjected to: (a) torsional and biaxial loading at infinite life **[27,28];** (b) uniaxial and biaxial loading at finite life **[29].**

Table 1. Infinite life fatigue tests: tensile loading condition **[27,28].**

TEST NO.	σ_a [MPa]	σ_m [MPa]	N_{exp} [cycles]	
T1	260	0	$2.46 \cdot 10^6$	Failed
T2	240	0	$1.20 \cdot 10^7$	Run-out
T3			$1.39 \cdot 10^6$	Failed
T4	220	0	$7.29 \cdot 10^5$	Failed
T5	200	0	$8.09 \cdot 10^6$	Failed
T6			$2.03 \cdot 10^5$	Failed
T7	180	0	$4.18 \cdot 10^6$	Failed
T8			$1.19 \cdot 10^7$	Run-out
T9	160	0	$2.72 \cdot 10^6$	Failed
T10			$1.20 \cdot 10^7$	Run-out
T11	140	0	$1.20 \cdot 10^7$	Run-out

Table 2. Infinite life fatigue tests: torsional loading condition **[27,28].**

TEST NO.	τ_a [MPa]	τ_m [MPa]	N_{exp} [cycles]	
T12	190	0	$9.76 \cdot 10^5$	Failed
T13			$8.80 \cdot 10^5$	Failed
T14			$7.77 \cdot 10^5$	Failed
T15			$1.66 \cdot 10^6$	Failed
T16	165	0	$1.00 \cdot 10^7$	Run-out
T17			$1.01 \cdot 10^7$	Run-out
T18			$1.00 \cdot 10^7$	Run-out

Table 3. Infinite life fatigue tests: biaxial loading condition **[27,28].**

TEST NO.	σ_a [MPa]	σ_m [MPa]	τ_a [MPa]	τ_m [MPa]	β [°]	N_{exp} [cycles]	
T19	300	-300	150	0	90	$1.34 \cdot 10^6$	Failed
T20	250	-250	125	0	90	$1.00 \cdot 10^7$	Failed
T21						$9.11 \cdot 10^5$	Failed
T22						$3.91 \cdot 10^6$	Failed
T23						$2.71 \cdot 10^6$	Failed
T24	225	-225	150	0	90	$9.93 \cdot 10^5$	Failed
T25						$1.12 \cdot 10^6$	Failed
T26						1.40·106	Failed
T27	200	-200	100	0	90	$9.17 \cdot 10^6$	Run-out
T28						$9.32 \cdot 10^6$	Failed
T29						$1.00 \cdot 10^7$	Run-out
T30						$1.00 \cdot 10^7$	Run-out
T31	187.5	-187.5	125	0	90	$1.00 \cdot 10^7$	Run-out
T32						$5.94 \cdot 10^6$	Failed
T33						$2.58 \cdot 10^6$	Failed
T34						$1.02 \cdot 10^7$	Run-out
T35	150	-150	100	0	90	$1.00 \cdot 10^7$	Run-out
T36	150	-150	75	0	90	$1.01 \cdot 10^7$	Run-out

Table 4. Static and fatigue properties of the two DCIs examined.

MATERIAL	σ_u [MPa]	$\sigma_{af,-1}$ [MPa]	$\tau_{af,-1}$ [MPa]	k	k^*	N_0 [cycles]
DCI EN-GJS-700-2	689	197	178	-	-	-
DCI EN-GJS-400-18	460	173	167	-0.078	-0.099	$2 \cdot 10^6$

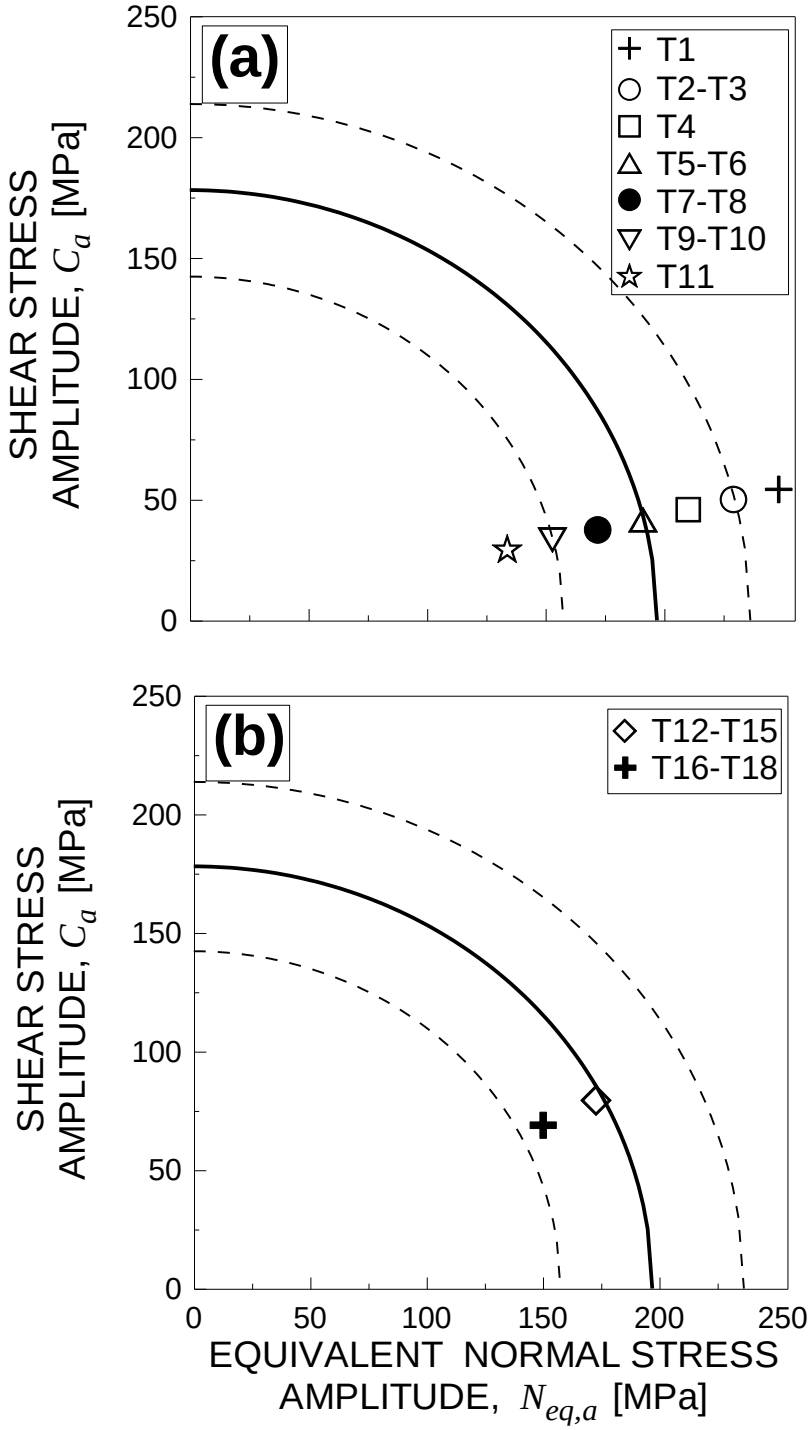

Figure 3. Fatigue endurance assessment for infinite life fatigue tests under: (a) tensile loading; (b) torsional loading **[27,28].**

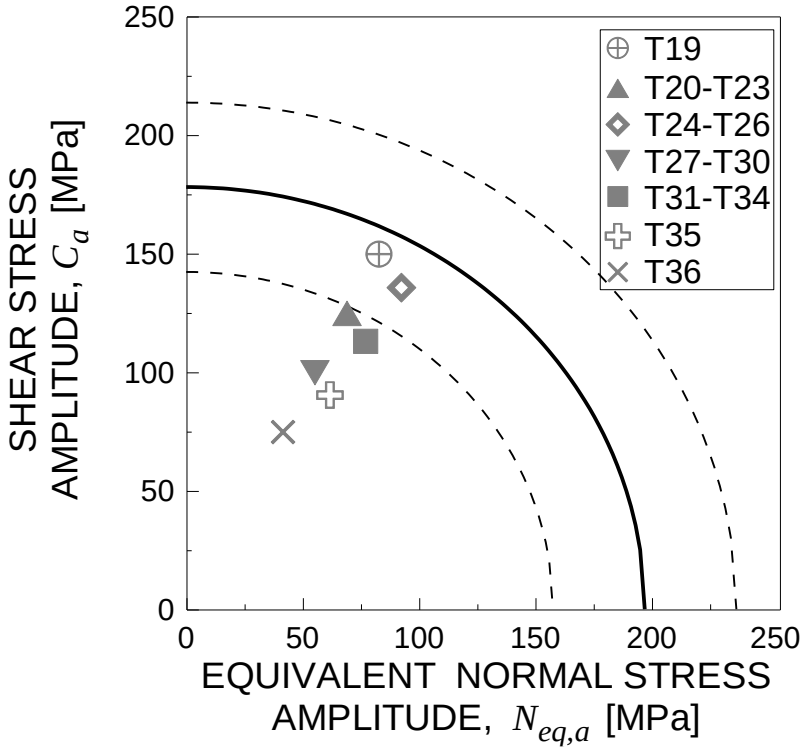

Figure 4. Fatigue endurance assessment for infinite life fatigue tests under biaxial loading **[27,28].**

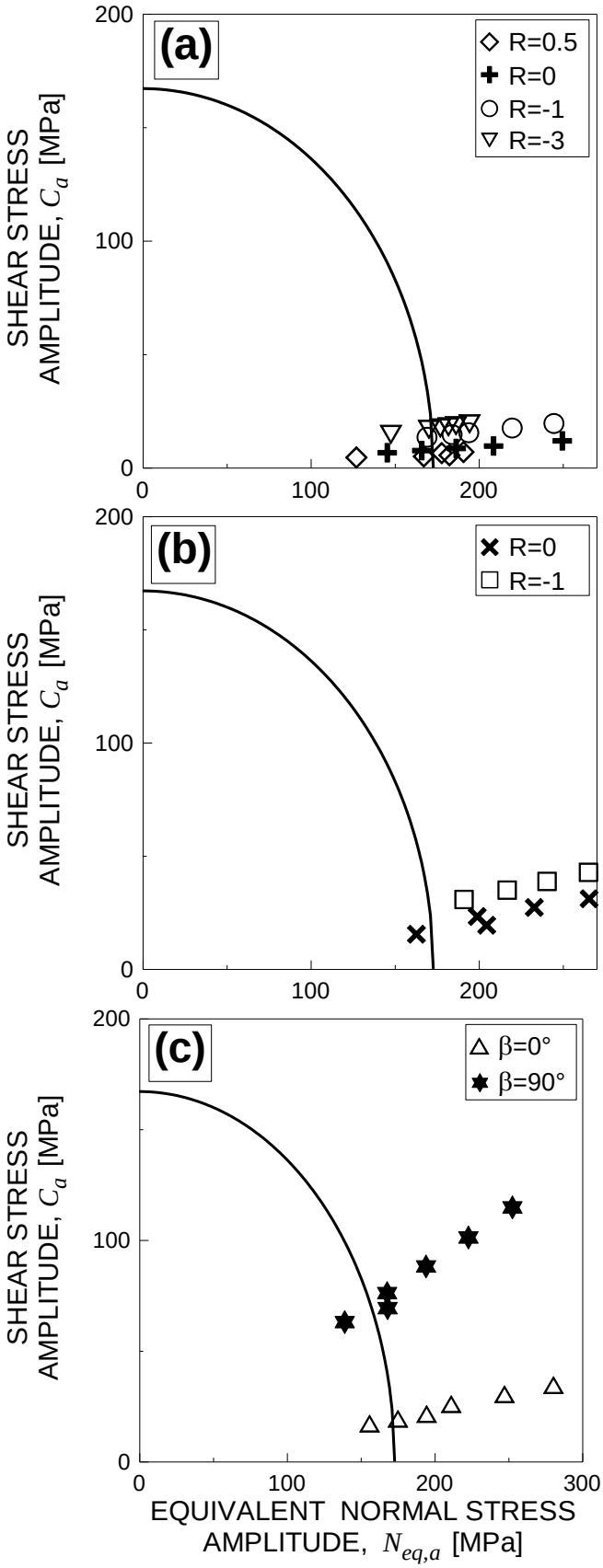

Figure 5. Fatigue endurance assessment for finite life fatigue tests under: (a) tensile loading; (b) torsional loading; (c) biaxial loading (R=-1) **[29].**

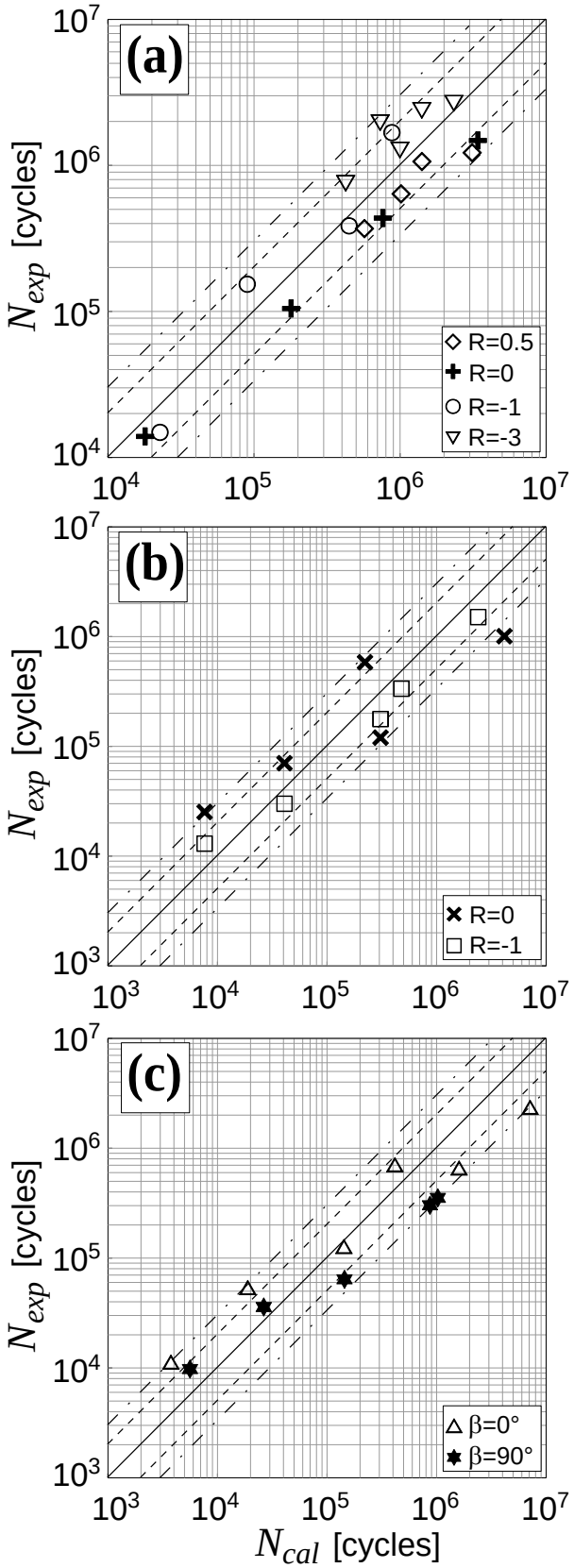

Figure 6. Comparison between experimental and computed fatigue life: (a) tensile loading; (b) torsional loading; (c) biaxial loading (R=-1) **[29].**

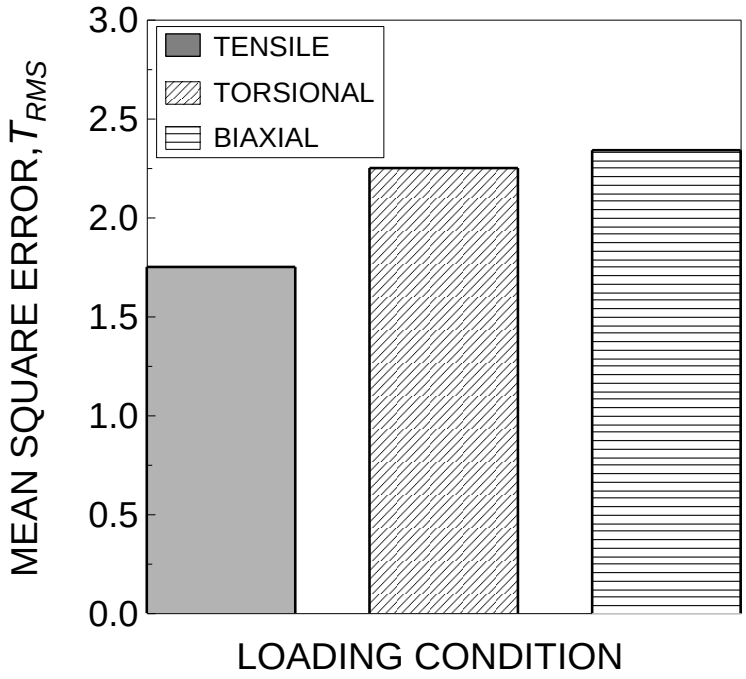

Figure 7. Mean square error computed for finite life fatigue tests **[29].**